Thermal migration of alloying agents in aluminium

S.P. Cooil,[1] E.A. Mørtsell,[1] F. Mazzola,[1] M. Jorge,[1] S. Wenner,[1]
M.T. Edmonds,[2] L. Thomsen,[3] H.W. Klemm,[4] G. Peschel,[4] A. Fuhrich,[4]
M. Prieto,[4] Th. Schmidt,[4] J.A. Miwa,[5] R. Holmestad,[1] and J.W. Wells[1,6,*]

[1]*Department of Physics, Norwegian University of Science and Technology (NTNU), N-7491 Trondheim, Norway*

[2]*School of Physics and Astronomy and Monash Centre for Atomically Thin Materials, Clayton Victoria 3800, Australia*

[3]*The Australian Synchrotron, 800 Blackburn Road, Clayton, Victoria 3168, Australia*

[4]*Department of Chemical Physics, Fritz-Haber Institute of the Max-Planck Society, Faradayweg 4-6 14195 Berlin, Germany*

[5]*Department of Physics and Astronomy, Interdisciplinary Nanoscience Center (iNANO), University of Aarhus, 8000 Aarhus C, Denmark*

[6]*Present address: Department of Chemistry and Physics, La Trobe University, Bundoora, Melbourne, Australia*

(Dated: October 11, 2016)

Abstract

The *in situ* thermal migration of alloying agents in an Al-Mg-Si-Li alloy is studied using surface sensitive photo-electron and electron diffraction/imaging techniques. Starting with the preparation of an almost oxide free surface (oxide thickness = 0.1 nm), the relative abundance of alloying agents (Mg, Li and Si) at the surface are recorded at various stages of thermal annealing, from room temperature to melting (which is observed at 550°C). Prior to annealing, the surface abundances are below the detection limit $\ll 1\%$, in agreement with their bulk concentrations of 0.423% Si, 0.322% Mg and 0.101% Li (atomic %). At elevated temperatures, all three alloying agents appear at drastically increased concentrations (13.3% Si, 19.7% Mg and 45.3% Li), but decrease again with further elevation of the annealing temperature or after melting. The temperature at which the migration occurs is species dependent, with Li migration occurring at significantly higher temperatures than Si and Mg. The mechanism of migration also appears to be species dependent with Li migration occurring all over the surface but Mg migration being restricted to grain boundaries.

Aluminium is one of the lightest and most abundant solid elements on earth, and has therefore attracted much attention for weight-conscious applications. In its pure elemental form, aluminium is a soft and malleable metal which is poorly suited to applications where strength is required. However, for more than a century, the inclusion of small quantities of alloying agents (in particular, magnesium and copper) has been shown to favorably modify aluminium's strength and hardness[1,2]. Whilst the initial development of aluminium alloys was driven by the need for light but strong airframes for lighter-than-air flight[3], aluminium alloys soon attracted attention for a wide range of weight-restrictive applications, including heavier-than-air flight, high performance motor vehicles, bicycles, and space vehicles. Very early on, aluminium alloys such as duralumin were also employed in medicine, notably as surgical splints and implants[1,4], where not only their weight and strength were important, but additionally, their low atomic number did not hinder diagnosis using the emergent X-ray radiographic techniques of the time[5]. Whilst radiology has developed dramatically over the last century, aluminium alloys are still of central importance; not only is their weight-to-strength ratio important, additionally their non-magnetic nature makes them well suited to high-field environments such as magnetic resonance imaging[6].

Whilst the alloying of aluminium began over a century ago, the parameter space is enormous and time consuming to explore. The wide choice in alloying agents (i.e. Cu, Mg, Mn, Si, Sn, Zn, Fe, Cr, V, Ti, Bi, Ga, Ge, Pb, Zr, Sc, and countless combinations thereof), mechanical processing treatments (i.e. deformation and work hardening) and thermomechanical treatments (i.e. heating time and rate, quenching and thermal cycling) all play an important role in the complex mechanisms responsible for the physical properties of the alloy. For example, in wrought alloys which have small amounts of Mg and Si as the main alloying agents (also known as 6000-series, or 6xxx, alloys) the strength has been shown to increase as a result of the aggregation of nano-sized metastable precipitate needles during age hardening, where the strength of the material usually peaks when the majority of the needles are of the so-called β'' type.[7]

Recently lithium has also attracted attention as a solute addition, as it is exceptionally lightweight and has been shown to improve the age-hardening response and thermal stability of Al alloys[8]. However it is believed that during the hardening process a significant proportion of Li migrates to the surface, leaving less Li available for the precipitation of hardening phases.[9] On the other hand, migration to surfaces and grain boundaries may be

advantageous for electrochemical applications and for corrosion resistance[10]. An extreme example of surface migration causing corrosion resistance is the formation of graphene from bulk impurities on a range of reactive metal surfaces[11,12], giving rise to a single-atom-thick inert and corrosion resistant coating with a broad range of potential applications[13,14]. It is therefore interesting to understand which bulk species agents migrate towards the surface and/or grain boundaries of the material and the thermal dependency of these mechanisms.

In this study we utilise experimental techniques based on photo-electron emission to study the migration of alloying agents during *in situ* thermal annealing. Specifically, we use X-ray photo-emission spectroscopy (XPS) and photo-emission electron microscopy (PEEM), supplemented by low energy electron microscopy (LEEM). These techniques are very surface sensitive[15,16] and are well suited to the study of light elements[17] and the spatial distribution of minority species[18], thus they are ideal for revealing the dynamics of surface migration in aluminium alloys.

A 4 kg cylindrical billet of an Al-Mg-Si-Li mix was cast and homogenized for three hours at 575°C before being air cooled to room temperature. The billet was preheated to about 540°C before extruding it as a round profile with a 20 mm diameter (for further details of the heat treatment, see Ref. 19). The abundance (atomic %) of the alloying agents in the Al-Mg-Si-Li alloy was measured by inductively coupled plasma optical emission spectroscopy and found to be 0.423(5)% Si, 0.322(3)% Mg, 0.101(1)% Li, 0.097(1)% Fe and 0.015(1)% Mn. A 1 mm thick disk was cut perpendicular to the extrusion direction and further machined to a square of 10×10 mm^2. The sample surface was polished with grade 4000 SiC paper prior to electro-polishing (using an electrolyte consisting of 70% ethanol, 10% 2-butoxyethanol, 8% perchloric acid and 12% distilled water). Samples were then introduced into an Ultra High Vacuum (UHV) chamber where XPS or PEEM/LEEM measurements were performed. Prior to measuring, samples were further cleaned *in situ* in UHV by sufficient cycles of Ar^+ bombardment to remove the surface oxide. Additional *in situ* annealing was also carried out, and is detailed below. XPS measurements were performed both using a home Mg-kα/Al-kα XPS instrument, and at the Soft X-ray endstation at the Australian Synchrotron[20]. For the PEEM/LEEM measurements we used the SMART instrument at the synchrotron light source "BESSY-2" of the Helmholtz-Center Berlin for Material and Energy (HBZ)[21].

Following the in-vacuum preparation and annealing to 200°C (for 5 min.), an XPS survey of the sample was conducted. Fig. 1a) shows an overview measurement which is dominated

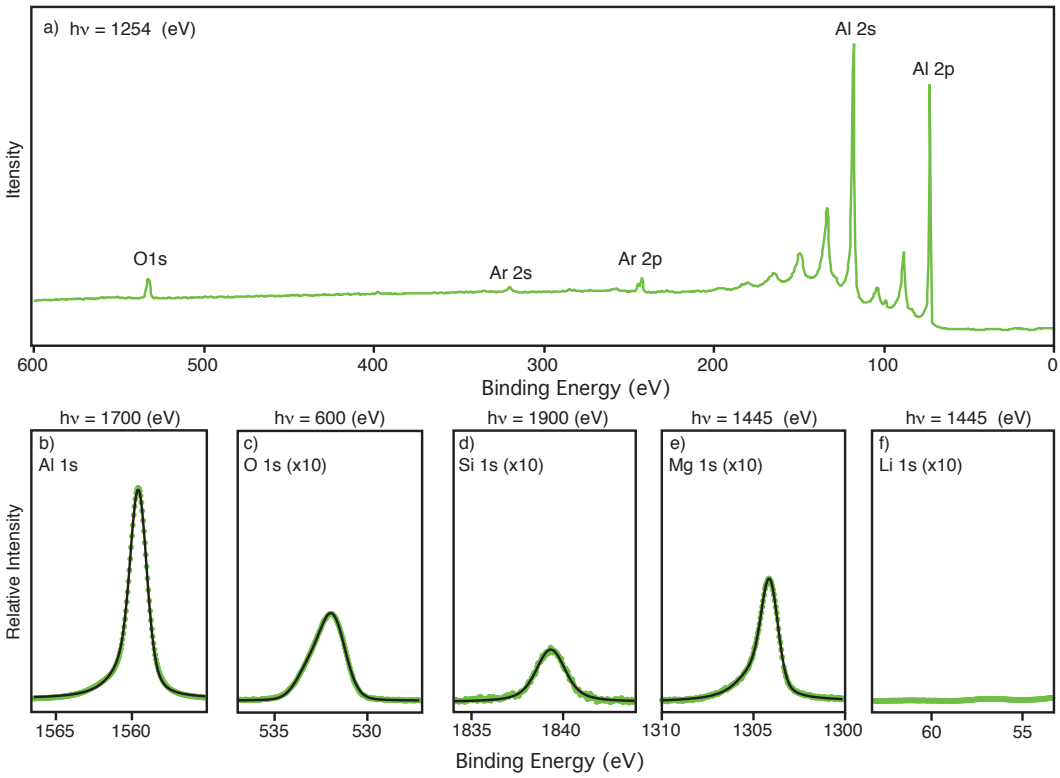

FIG. 1. (Color online) Synchrotron XPS measurements of an Ag-Mg-Si-Li alloy which has been prepared by *in situ* argon ion sputtering and annealing to 200°C. a) Photoemission survey spectra using photon energy $h\nu$=1254 eV. b-f) Detailed core level spectra for Al 1s, O 1s, Si 1s, Mg 1s and Li 1s respectively. The measured intensities (green markers) are shown following Shirley background subtraction, and fitted with Voigt functions (magenta lines), from which the peak area is extracted. The peaks are scaled by cross section and normalized to the intensity of the Al 1s photoelectron peak, thereby revealing the relative surface abundances; Al:Si:Mg:Li = $1:0.02:0.05:0.00$. The oxygen peak is due to incomplete removal of the surface oxide; ≈0.1 nm remains. The kinetic energy of all photoelectron peaks is maintained at ≈140 eV to ensure similar escape depth of the emitted electrons.

by the Al 2p and 2s core levels peaks and their rich plasmon loss structures. Small O 1s, Ar 2s and Ar 2p core levels peaks are also indicated in the spectra and are present as a result of Ar^+ sputtering and incomplete oxide removal. Using the assumption that the oxide is surface localised, this peak intensity corresponds to an oxide thickness of 0.1 nm. However, it is also conceivable that some of the oxide detected is dissolved in the bulk alloy, or has

migrated to grain boundaries. If this is indeed the case, then the above assumption that the oxide is localised at the surface would result in an overestimation of the surface oxide thickness.

Detailed 1s core levels of Al, O, Si, Mg and Li were also collected using a range of photon energies (Fig. 1b-f). The photon energy was selected such that the kinetic energy of the escaping photo-electron was ≈140 eV for each acquisition, thus maximising the surface sensitivity. 1s (singlet) core levels, lacking plasmon loss structures, were acquired to facilitate improved modeling; for each dataset, the core level peak has been modeled as Voigt contributions atop a Shirley background. As can be seen in the figure, the agreement between the model and measurement is excellent.

The measurements and peak analysis presented in Fig. 1 allow a quantitative understanding of the species present near the sample surface (i.e. within ≈1 nm). This is exemplified by the Li 1s core level, which is below the detection limit, thus indicating that a negligible amount of Li is localised at the surface. Unlike Li, the alloying agents Si and Mg are both present with detectable and significant abundances (≈ 2% and 5%, respectively). In other words, the quantity of Si and Mg located near the surface is approximately an order of magnitude larger than the bulk abundances of Al:Si:Mg:Li = 1 : 0.004 : 0.003 : 0.001, indicating that at 200°C significant surface segregation of Si and Mg has already occurred and that surface segregation of Li has not.

In order to observe the thermal dependence of the segregation, we have performed similar measurements and analysis following annealing for 5 min. to a wide range of temperatures (from 25°C to 500°C)[22]. Fig. 2 shows the abundance of surface Mg, Li and Si (plotted relative to Al) as the annealing temperature is increased. For low temperatures (i.e. upto 120°C), the surface abundance of all three alloying agents is below the detection limit (consistent with the bulk concentrations). In the range 150°C to 450°C, Mg and Si migrate to the surface, with a maximum surface abundance of Mg 19.7% and Si 13.3% observed at 280°C. At higher temperatures, Mg completely redissolves into the bulk, with Mg → 0% at 450°C and Si partially redissolves with Si → 6.0% at 500°C.

The thermal migration of Li is somewhat different; below the relatively high temperature of 300°C, no surface Li is detected. Above this temperature, Li migrates to the surface extremely readily, resulting in a surface abundance of 45.3% (relative to Al) – an astounding amount considering that the initial bulk concentration was only 0.1%. Above 400°C, the

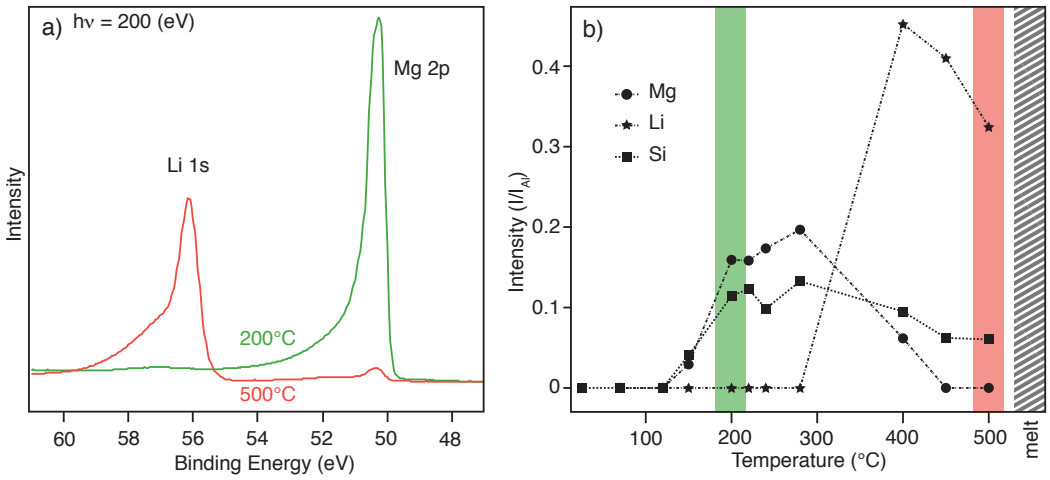

FIG. 2. (Color online) Thermal evolution of surface species. a) The Li 1s and Mg 2p core levels at two selected temperatures (not normalised to cross-section). b) The surface concentrations of Mg, Li and Si (indicated by circles, stars and squares, respectively), extracted from XPS measurements, during annealing from room temperature to 500°C. The green and red bands indicate the temperatures at which the data in panel a) are recorded.

surface abundance of Li is somewhat reduced, but still remains *very* high.

In order to understand the spatial distribution of the alloying agents at the surface, LEEM and PEEM were used. Bright-field LEEM images were collected using SV=5.5 eV, where SV is the 'start voltage', or potential of the sample relative to the incident electrons. This allows the polycrystalline nature of the material to be clearly observed; in Fig. 3a) we show such an image in which a grain boundary triple-point is visible. Micro-diffraction patterns were collected from the three grains, and reveal that they are all close to {100} orientation, but individually tilted with respect to the sample surface; i.e. forming a pyramid-like geometry.

As with the XPS measurements presented above, the LEEM/PEEM allows *in situ* control of sample temperature. Measurements were made following a range of thermal annealing steps – as described for the XPS experiment. Fig. 3b shows an image formed using photo-emitted electrons; both the photon energy $h\nu$ and kinetic energy E_K of the emitted electron can be selected such that a particular binding energy E_B is probed ($E_B = h\nu - E_K$). Since E_B is element specific, this allows chemical-sensitive mapping and spectroscopy to be performed. In Fig. 3 we focus on the 400°C annealing step; according to the XPS study, this corresponds to a temperature at which Li, Mg and Si are abundant at the surface (Fig. 2). A

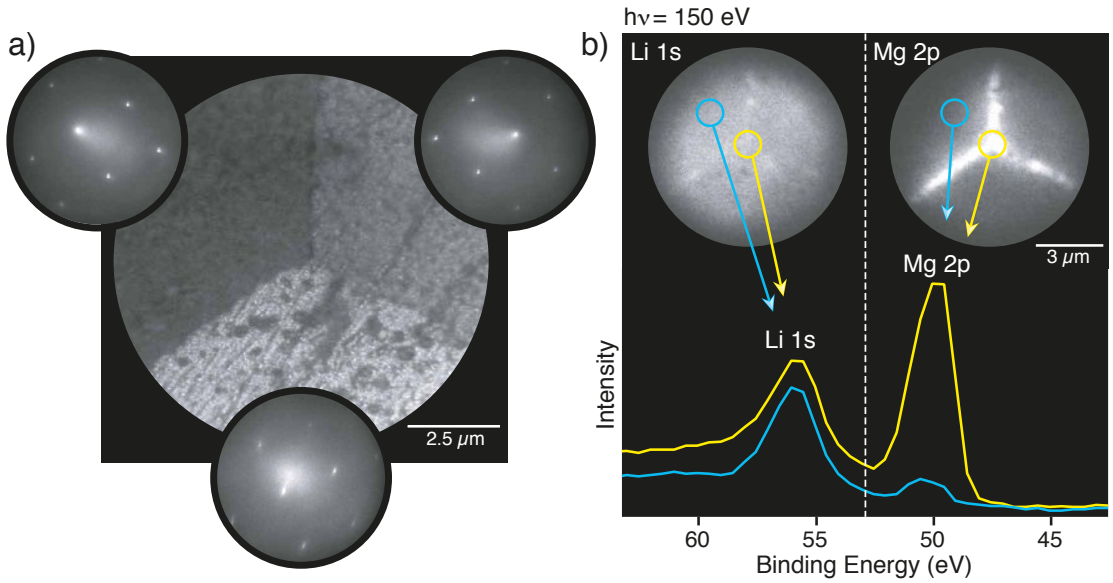

FIG. 3. (Color online) LEEM, LEED and PEEM study of a grain boundary following an *in situ* anneal of the sample to 400°C. a) Bright field LEEM image of the grain boundary (SV=5.5 eV). Contrast in each grain boundary is visible due to the different projections of the 0,0 diffraction spot in the micro-LEED patterns (shown as inserts for each grain). b) Images and spectra extracted from a series of PEEM images (ΔSV=0.5 eV) covering the kinetic energy range of the Li 1s and Mg 2p core levels. Upper panel; images formed using the peak intensity from the Li 1s and Mg 2p peak signals (left and right, respectively. Lower panel; Spectra extracted from within the grain boundary (yellow) and the grain surface (cyan).

large series of PEEM images were formed using constant photon energy ($h\nu$=150 eV) whilst SV is incrementally increased (equivalent to sweeping E_K), thus each image is sensitive to an incrementally different E_B (in the range E_B =40 to 65 eV). From such a dataset, it is straightforward to extract either a spatial image of a particular E_B (i.e. Fig. 3b, upper panel), or to extract spectral information (i.e. intensity of emitted electrons *vs.* E_B) for a specific position within the image (i.e. Fig. 3b lower panel). The two images we present in Fig. 3b correspond to the Li and Mg core-levels. Whereas the image formed using the Li 1s peak has high intensity relatively uniformly distributed across the surface, indicating that Li is ubiquitous, the image formed using the Mg 2p peak shows very high intensity specifically at the grain boundaries. This observation is additionally supported by the spectroscopic measurements: the lower panel shows that large Li and Mg peaks are observed at the grain

boundary intersection (yellow data and yellow circle), whereas away from the boundaries, a similar quantity of Li is present but Mg is much reduced (cyan data and cyan circle). We therefore infer that, whilst these alloying agents both migrate to the surface during annealing, the mechanism is somewhat different; Mg is predominantly observed at the grain boundaries, whereas Li is ubiquitous.

A close observation of the Li 1s and Mg 2p intensity maps reveals some bright and dark spots at the grain boundary. Interestingly, these regions correlate to regions of increased oxide, and probably indicate the presence of small inclusions of Mg and/or Li oxides at the grain boundary.

In order to observe the redissolving of alloying agents from the surface, we have also conducted XPS measurements at the melting temperature. In Fig. 4, XPS measurements are shown after melting (which was observed at 550°C), and are compared with measurements from the initial (not annealed) surface. Not surprisingly, the Mg is essentially absent. Already prior to melting, the Mg surface concentration was observed to return to its initial value of ≈0 (see Fig. 2b), indicating that the Mg was fully redissolved at high temperatures prior to melting. In addition to this, the surface abundance of both Li and Si also reduce after melting. In Fig. 2b, significant concentrations of both Li and Si were observed at T=500°C (i.e. just below the melting point) – however on melting, the concentrations return to their initial values of ≈0. In fact, after melting, the only core level observed in Fig. 4 is Al 2p. One can also observe that, whilst the total area of the Al 2p core level is not significantly changed, the high binding energy shoulder ($E_B \approx 77$ eV) has grown into a more distinct peak. This component corresponds to oxidised aluminium; this oxidation has occurred during the melting experiment and may simply be due to a worsening of the base vacuum when melting the sample ($p \approx 5 \times 10^{-9}$ mbar), or may be due to bulk dissolved oxygen migrating to the surface. Although the oxide component is large compared to the initial surface, it is worth restating that these measurements are especially surface sensitive. In fact, this oxide component corresponds to a surface oxide layer only 0.37 nm thick (c.f. 0.10 nm initially).

In conclusion, we have demonstrated that the combination of XPS and LEEM/PEEM is a powerful approach for studying the surface migration of alloying agents during *in situ* annealing at a wide range of temperatures from room temperature to melting at 550°C. Surface sensitive XPS, LEEM and PEEM measurements reveal both spectroscopic and spatial

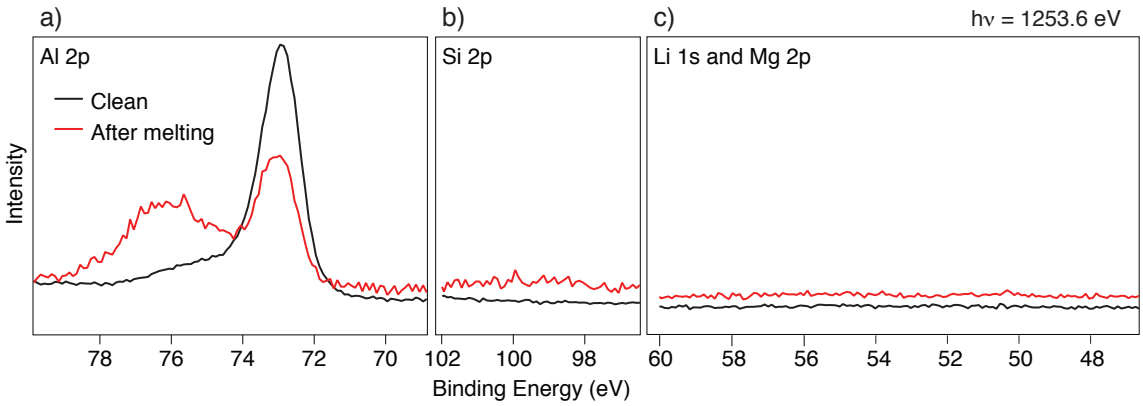

FIG. 4. (Color online) XPS measurements of the clean Al-Mg-Si-Li sample prior to annealing (black curves) and after annealing to the melting point ($T = 550$°C, red curves). a) The Al 2p region showing that the surface oxide (component at $E_B \approx 77$ eV) has increased during the melting. b) The Si 2p region and c) the Li 1s and Mg 2p region showing that these species are below the detection limit.

information of the migration processes in an Al-Mg-Si-Li alloy. Dramatic migration of Mg, Si and Li to the surface is observed – with the surface contributions increasing by more than 2 orders of magnitude above their initial (bulk) concentrations. For the case of Li, the initial concentration is ≈0.1%, but rises to 45.3% at the surface following annealing to 400°C. The surface migration is somewhat reversible; at higher temperatures, Mg is completely redissolved into the bulk whereas the surface concentrations of Si and Li reduce, but remain high compared to the initial values. On melting (at $T = 550$°C), the surface abundance of Si and Li also return to their initial values, either due to redissolving into the bulk, although loss of Li via evaporation is also a possibility. PEEM/LEEM measurement further reveal that the surface migration is not the same for all species; Mg migration is dominated by grain boundaries whereas Li is observed across the entire surface. Since the abundance of each species at the surface/grain-boundary follows its own temperature dependence, we speculate that it will be possible to control the surface termination of these alloys by careful control of the annealing temperature. More specifically, susceptibility to inter-granular corrosion is reduced when the grain boundaries are enriched by Mg[23]. Thus it should be possible to find the maximum corrosion resistance for Mg-based alloys by optimising the Mg concentration at grain boundaries using the annealing temperature. Determining when the alloying agents have diffused to the surface during annealing can alter the physical properties of the

material to a large extent. The Si:Mg ratio within the grains will be influenced by surface migrations, and is very important for the formation of the nanosized precipitate phases during hardening. Low Si:Mg ratios typically suppress the formation of the phases promoting strength, and the alloy becomes softer than in regions with higher Si:Mg ratios[24]. Li depletion also leaves less solute available for the precipitation of hardening phases, rendering the material softer than in regions with more Li[8]. By documenting at which temperature Li depletion occurs, this effect can readily be avoided. We conclude that *in situ* annealing and surface sensitive photo-emission methods are able to provide a wealth of information on the migration of alloying agents in solid light metal alloys such as Al-Mg-Si-Li, which will be important for thermomechanical treatments intended for optimising the physical properties of the alloys, and will give essential information for tailoring new alloys.

Acknowledgments: The project has been supported through the BIA RolEx project (No. 219371) by Hydro Aluminium and the Research Council of Norway. This research was partially undertaken on the soft X-ray beamline at the Australian Synchrotron (AS), Victoria, Australia and partially at the SMART beamline at 'BESSY' in the Helmholtz Zentrum, Berlin (HZB); we thank AS and HZB for the allocation of synchrotron time and for technical support.

APPENDIX: High kinetic energy 1s cross-sections for the solid light elements

It is common practice in quantitative photo-emission studies to use the calculations by Yeh and Lindolf[25] to estimate the photo-ionisation cross-sections. As well as the original paper, these calculations form the backbone of several more recent analysis tools, and are available in a widely used, convenient online resource[26]. However, in both the original paper, and the website, the calculations are only evaluated in the energy range $h\nu < 1500$ eV. As high energy XPS becomes more available, there is an increasing need for providing cross-section data for higher photon energies. For example, in this work, we have acquired core level data at photon energies up to 1980 eV.

More specifically, for this work, an estimate of the photo-ionisation cross-section is needed for Al 1s and Si 1s at $h\nu$ =1700 and $h\nu$ =1980 eV, respectively. The binding energies of these core levels are outside of the energy range considered by Yeh and Lindolf[25]. To overcome this problem, we first investigate the functional form of the 1s cross-sections for solid light elements in general.

Although the functional form of the cross-section may be more complex at low photon energy, the high energy tail can be well approximated as an exponential decay. This is evident in Fig. 5, where the 1s cross-sections are plotted for elements z =3 to 14 (Li to Si). For z =3 to 12 (Li to Mg), the cross-sections from Refs. 25 and 26 are plotted (dashed lines) for the energy range $h\nu < 1500$ eV. These plots are overlaid by simple exponential decays for the energy range $h\nu$ =1000 to 2500 eV, by thick solid curves of matching colour. In the range $h\nu$ =1000 to 1500 eV, both the calculated cross-section and the exponential decay co-exist. As can be seen in the Fig. 5, the match is extremely close and the thick trace of each exponential decay sits directly on top of the underlying dashed line.

In Fig. 5, we have chosen to plot the exponential decay in the form:

$$\chi_z = y_{0,z} + A_z \exp\left\{\frac{-(h\nu - 1000)}{\tau_z}\right\} \tag{1}$$

where z is the atomic number, χ_z is the cross-section and $y_{0,z}$, A_z and τ_z are element specific constants found by fitting the exponential function to the literature cross-sections (in the energy range $h\nu$ =1000 to 1500). The extracted values of $y_{0,z}$ and A_z and are tabulated in table I. In all cases, τ_z was found to be 330.63. The cross-section can only be estimated in this way for elements up to Mg (z=12), because Ref. 25 does not contain calculations for the

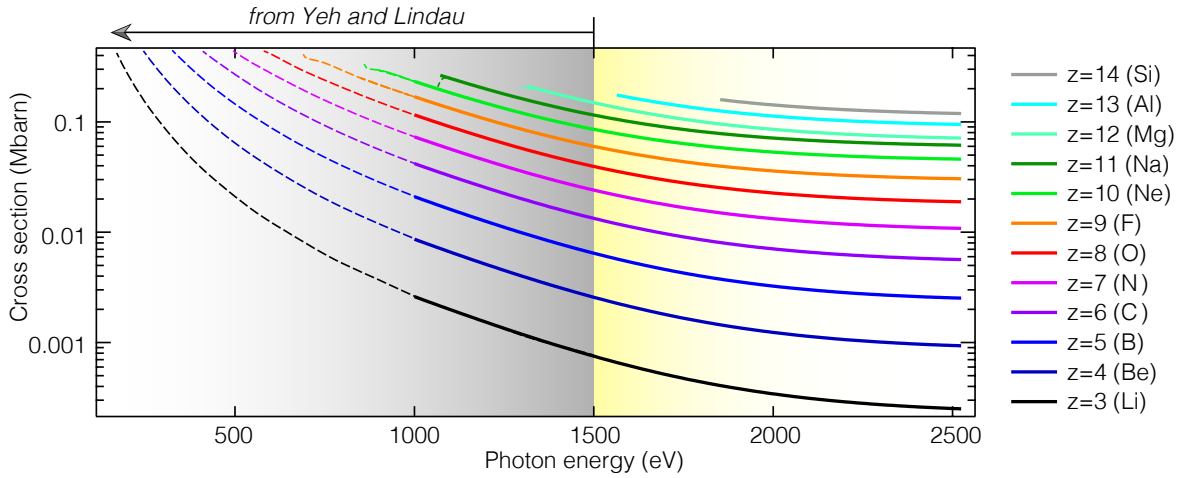

FIG. 5. (Color online) Calculated and extrapolated photo-ionisation cross-sections of the 1s orbitals of elements z =3 to 14. Dashed lines show the values calculated by Yeh and Lindau[25] (available only for $h\nu < 1500$ eV). Thick solid lines overlap with the calculated values in the range $1000 < h\nu < 1500$, and are extrapolated to higher energy.

1s orbital of heavier elements. Instead we observe that $y_{0,z}$ and A_z both follow a power-law dependence with z, i.e. $y_{0,z} \propto z^n$ and $A_z \propto z^m$. This makes it straightforward to extrapolate the coefficients in table I for z =13 and 14, and so to estimate the 1s high-photon-energy photo-ionisation cross-section for elements $z \geq 13$, which are not included in Ref. 25. This extrapolation method is consistent with the related study by Verner and Yakovlev[27].

TABLE I. Values of $y_{0,z}$ and A_z for $z = 3$ to 14. In all cases, $\tau_z = 330.63$. For $z = 3$ to 12, these values are found by fitting an exponential decay to the calculations of Yeh and Lindau[25] in the energy range $1000 < h\nu < 1500$. For $z = 13$ and 14, these (italicised) values are extrapolated from the corresponding constants for the lighter elements.

element	z	$Y_{0,z}$	A_z
Li	3	0.0002267	0.0023805
Be	4	0.00085627	0.0077799
B	5	0.0023396	0.018637
C	6	0.0052806	0.036592
N	7	0.01019	0.063029
O	8	0.017888	0.097847
F	9	0.029097	0.14007
Ne	10	0.04407	0.18863
Na	11	0.058946	0.25565
Mg	12	0.067623	0.36963
Al	*13*	*0.090078*	*0.46876*
Si	*14*	*0.11301*	*0.60572*

* quantum.wells@gmail.com

[1] S. Melville, "Demonstration of "duralumin."," Proceedings of the Royal Society of Medicine **6**, 161 (1913), URL http://www.ncbi.nlm.nih.gov/pmc/articles/PMC2006514/.

[2] R. Woodward, "Recent developments in light alloys," NASA Technical Reports **NACA-TM-3**, 93R10024 (1920).

[3] D. Robinson, *Giants in the Sky: A History of the Rigid Airship* (University of Washington Press;, 1973), 1st ed.

[4] E. M. Little, "A lecture on a new material (duralumin) for surgical appliances: Delivered at the medical graduates' college and polyclinic," British Medical Journal **1**, 236 (1912), URL http://www.ncbi.nlm.nih.gov/pmc/articles/PMC2344469/.

[5] T. H. Bryce, "Certain points in the anatomy and mechanism of the wrist-joint reviewed in the light of a series of Røntgen ray photographs of the living hand," Journal of Anatomy and Physiology **31**, 59 (1896), URL http://www.ncbi.nlm.nih.gov/pmc/articles/PMC1327812/.

[6] H. Elhawary, A. Zivanovic, B. Davies, and M. Lampérth, "A review of magnetic resonance imaging compatible manipulators in surgery," Proceedings of the Institution of Mechanical Engineers, Part H: Journal of Engineering in Medicine **220**, 413 (2006), http://pih.sagepub.com/content/220/3/413.full.pdf+html, URL http://pih.sagepub.com/content/220/3/413.abstract.

[7] C. D. Marioara, H. Nordmark, S. J. Andersen, and R. Holmestad, "Post-β'' phases and their influence on microstructure and hardness in 6xxx Al-Mg-Si alloys," Journal of Materials Science **41**, 471 (2006), ISSN 1573-4803, URL http://dx.doi.org/10.1007/s10853-005-2470-1.

[8] Y. Koshino, M. Kozuka, S. Hirosawa, and Y. Aruga, "Comparative and complementary characterization of precipitate microstructures in Al–Mg–Si(–Li) alloys by transmission electron microscopy, energy dispersive x-ray spectroscopy and atom probe tomography," Journal of Alloys and Compounds **622**, 765 (2015), ISSN 0925-8388, URL http://www.sciencedirect.com/science/article/pii/S0925838814026371.

[9] H. J. Leighly and P. G. Coleman, "Vacancy clustering in quenched Al-Li solid solution alloys studied by doppler broadening spectroscopy," Journal of Physics: Condensed Matter **10**, 10423 (1998), ISSN 0953-8984, URL http://stacks.iop.org/0953-8984/10/i=46/a=010.

[10] M. Hurlen Larsen, J. C. Walmsley, O. Lunder, and K. Nisancioglu, "Effect of heat treatment on grain boundary nanostructure and corrosion of low copper AlMgSi alloy," ECS Transactions **3**, 167 (2007), URL http://ecst.ecsdl.org/content/3/31/167.

[11] J. W. May, "Platinum surface LEED rings," Surface Science **17**, 267 (1969), URL http://www.sciencedirect.com/science/article/pii/0039602869902271.

[12] J. Wintterlin and M.-L. Bocquet, "Graphene on metal surfaces," Surface Science **603**, 1841 (2009), ISSN 0039-6028, special Issue of Surface Science dedicated to Prof. Dr. Dr. h.c. mult. Gerhard Ertl, Nobel-Laureate in Chemistry 2007, URL http://www.sciencedirect.com/science/article/B6TVX-4VCH6T7-3/2/6586fbab9f367324b38146b06f401fd8.

[13] L. Nilsson, M. Andersen, R. Balog, E. Lægsgaard, P. Hofmann, F. Besenbacher, B. Hammer, I. Stensgaard, and L. Hornekær, "Graphene coatings: Probing the limits of the one atom thick protection layer," ACS Nano **6**, 10258 (2012).

[14] F. Mazzola, T. Trinh, S. Cooil, E. R. Østli, K. Høydalsvik, E. T. B. Skjønsfjell, S. Kjelstrup, A. Preobrajenski, A. A. Cafolla, D. A. Evans, et al., "Graphene coatings for chemotherapy: avoiding silver-mediated degradation," 2D Materials **2**, 025004 (2015), URL http://stacks.iop.org/2053-1583/2/i=2/a=025004.

[15] M. P. Seah and W. A. Dench, "Quantitative electron spectroscopy of surfaces: A standard data base for electron inelastic mean free paths in solids," Surface and Interface analysis **1**, 2 (1979).

[16] J. A. Miwa, P. Hofmann, M. Y. Simmons, and J. W. Wells, "Direct measurement of the band structure of a buried two-dimensional electron gas," Phys. Rev. Lett. **110**, 136801 (2013).

[17] S. P. Cooil, J. W. Wells, D. Hu, Y. R. Niu, A. A. Zakharov, M. Bianchi, and D. A. Evans, "Controlling the growth of epitaxial graphene on metalized diamond (111) surface," Applied Physics Letters **107**, 181603 (2015), URL http://scitation.aip.org/content/aip/journal/apl/107/18/10.1063/1.4935073.

[18] S. P. Cooil, F. Mazzola, H. W. Klemm, G. Peschel, Y. R. Niu, A. Zhakarov, A. Evans, T. Schmidt, M. Y. Simmons, J. A. Miwa, et al., "In-situ patterning of ultra sharp dopant profiles in silicon," *in preparation* (2016).

[19] E. Mørtsell, C. Marioara, S. Andersen, J. Røyset, O. Reiso, and R. Holmestad, "Effects of germanium, copper, and silver substitutions on hardness and microstructure in lean Al-Mg-Si alloys," Met. Trans. A, (2015).

[20] B. C. C. Cowie, A. Tadich, and L. Thomsen, "The current performance of the wide range

(90–2500 ev) Soft X-ray Beamline at the Australian Synchrotron," AIP Conference Proceedings **1234**, 307 (2010), URL http://scitation.aip.org/content/aip/proceeding/aipcp/10.1063/1.3463197.

[21] T. Schmidt, U. Groh, R. Fink, E. Umbach, O. Schaff, W. Engel, B. Richter, H. Kuhlenbeck, R. Schlögl, H.-J. Freund, et al., "XPEEM with energy-filtering: advantages and first results from the SMART project," Surface Review and Letters **9**, 223 (2002).

[22] Note1, After annealing at higher temperatures, the sample is allowed to cool to $\approx 150°C$, in order to carry out XPS measurements.

[23] J. Holmestad, "(scanning) transmission electron microscopy studies of grain boundary segregation relevant to intergranular corrosion in Al-Mg-Si-Cu alloys," Doctoral thesis, http://hdl.handle.net/11250/283573 (2015).

[24] M. Torsæter, H. S. Hasting, W. Lefebvre, C. D. Marioara, J. C. Walmsley, S. J. Andersen, and R. Holmestad, "The influence of composition and natural aging on clustering during preaging in al–mg–si alloys," Journal of Applied Physics **108**, 073527 (2010), URL http://scitation.aip.org/content/aip/journal/jap/108/7/10.1063/1.3481090.

[25] J. J. Yeh and I. Lindau, "Atomic subshell photoinoization cross sections and asymmetry parameters: $1 \leq Z \leq 103$," Atomic Data and Nuclear Data Tables **32**, 1 (1985).

[26] URL https://vuo.elettra.eu/services/elements/WebElements.html.

[27] D. A. Verner and D. G. Yakovlev, "Analytic fits for partial photoionization cross sections," Astrophysical Applications of Powerful New Databases, ASP Conference series **78**, 57 (1995).